CONCLUSION

SPECT imaging of brain perfusion is more sensitive than EEG and MRI in the evaluation of central nervous system involvement in SLE. In the SPECT findings, cerebral cortices, especially the parietal, temporal and frontal lobes, are the most common sites to be involved in neuropsychiatric SLE patients. Furthermore, with the improvement of SPECT resolution, detection of the deep-seated structure in the brain has become possible. We found that involvement of basal ganglion is also not uncommon while the thalamus and the cerebellum are less involved in neuropsychiatric SLE. In the future, we believe that functional brain SPECT will play an increasingly important role in evaluating CNS conditions in patients with SLE.

REFERENCES

1. Van Dam AP. Diagnosis and pathogenesis of CNS lupus. *Rheumatol Int* 1991;11:1–11.
2. Ellis SG, Verity MA. The central nervous system involvement in systemic lupus erythematosus. A review of neuropathologic findings in 57 cases, 1955–1977. *Semin Arthritis Rheum* 1979;8:212–221.
3. Klippel JH, Zvaifler NJ. Neuropsychiatric abnormalities in systemic lupus erythematosus: an overview. *Semin Arthritis Rheum* 1986;15:185–199.
4. Carbott RM, Denburg SD, Denburg JA. Prevalence of cognitive impairment in systemic lupus erythematosus. *J Nerv Ment Dis* 1986;174:357–364.
5. Gaylis NB, Altman RD, Ostrov S, et al. The selective value of computed tomography of the brain in the cerebritis due to SLE. *J Rheumatol* 1982;9:850–854.
6. O'Connor P. Diagnosis of central nervous system lupus. *Canadian J Neurosci* 1988;15:257–260.
7. Nossent JC, Hovestadt A, Schonfeld DHW, Swaak AJG. Single-photon emission computed tomography of the brain in the evaluation of cerebral lupus. *Arthritis Rheum* 1991;34:1397–1403.
8. Vermess M, Bernstein RM, Bydder GM, Steiner RE, Young IR, Hughes GRV. Nuclear magnetic resonance imaging of the brain in systemic lupus erythematosus. *J Comput Assist Tomogr* 1983;7:461–467.
9. Stoppe G, Wildhagen K, Seidel JW, et al. Positron emission tomography in neuro-psychiatric lupus erythematosus. *Neurology* 1990;40:304–308.
10. Carbotte RM, Denburg SD, Denburg JA, Nahmias C, Garnett ES. Fluctuating cognitive abnormalities and cerebral glucose metabolism in neuropsychiatric systemic lupus erythematosus. *J Neurol Neurosurg Psychiatry* 1992;55:1054–1059.
11. Perani D, di Piero V, Vallar G, et al. Technetium-99m-HMPAO SPECT study of regional cerebral perfusion in early Alzheimer's disease. *J Nucl Med* 1988;29:1507–1514.
12. Stefan H, Kuhnen C, Biersack HJ, et al. Initial experience with ^{99m}Tc-HMPAO SPECT in patients with focal epilepsy. *Epilepsy Res* 1987;1:134–138.
13. Lewis SW, Ford RA, Syed GM, et al. A controlled study of ^{99m}Tc-HMPAO single-photon emission imaging in chronic schizophrenia. *Psychol Med* 1992;22:27–32.
14. Pozzilli C, Passafiume D, Bernardi S. SPECT, MRI and cognitive functions in multiple sclerosis. *J Neurol Neurosurg Psychiatry* 1991;54:110–115.
15. Meyer MA. Focal high uptake of HMPAO in brain perfusion studies: a clue in the diagnosis of encephalitis. *J Nucl Med* 1990;31:1094–1098.
16. Isshi K, Hirohata S, Hashimoto T, Miyashita H. Systemic lupus erythematosus presenting with diffuse low density lesions in the cerebral white matter on computed axial tomography scans: its implication in the pathogenesis of diffuse central nervous system lupus. *J Rheumatol* 1994;21:1758–1762.
17. Rubbert A, Marienhagen J, Pirner K, et al. Single-photon emission computed tomography analysis of cerebral blood flow in the evaluation of central nervous system involvement in patients with systemic lupus erythematosus. *Arthritis Rheum* 1993;36:1253–1262.
18. Kodama K, Okada S, Hino T, et al. Single-photon emission computed tomography in systemic lupus erythematosus with psychiatric symptoms. *J Neurol Neurosurg Psychiatry* 1995;58:307–311.
19. Emmi L, Bramati M, Cristofaro MTR, et al. MRI and SPECT investigations of the CNS in SLE patients. *Clin Exp Rheumatol* 1993;11:13–20.
20. Hughes RAC. Pathogenesis of neurological involvement in SLE. *Lancet* 1994;343:580–581.
21. Hanly JG, Walsh NMG, Sangalang V. Brain pathology in systemic lupus erythematosus. *J Rheumatol* 1992;19:732–741.
22. Devinsky O, Petito CK, Alonso DR. Clinical and neuropathological findings in systemic lupus erythematosus: the role of vasculitis, heart emboli and thrombotic thrombocytopenia purpura. *Ann Neurol* 1988;23:380–384.
23. Colamussi P, Giganti M, Cittant C, et al. Brain single-photon emission tomography with ^{99m}Tc-HMPAO in neuropsychiatric systemic lupus erythematosus: relations with EEG and MRI findings and clinical manifestations. *Eur J Nucl Med* 1995;22:17–24.
24. Szer IS, Miller JI, Rawlings D, et al. Cerebral perfusion abnormalities in children with central nervous system manifestations of lupus detected by single photon emission computed tomography. *J Rheum* 1993;20:2142–2147.
25. Aisen AM, Gabrielsen TO, McCune WJ. MR imaging of systemic lupus erythematosus involving the brain. *AJR* 1985;144:1027–1031.
26. McCune WJ, MacGuire A, Aisen A, Gebarski S. Identification of brain lesions in neuropsychiatric systemic lupus erythematosus by magnetic resonance scanning. *Arthritis Rheum* 1988;31:159–166.
27. Miller DH, Ormerod IEC, Gibson A, duBoulay EPGH, Rudge P, McDonald W. MR brain scanning in patients with vasculitis: differentiation from multiple sclerosis. *Neuroradiology* 1987;29:226–231.
28. Szer IS, Miller JH, Rawlings D, Shaham B, Bernstein B. Cerebral perfusion abnormalities in children with central nervous system manifestations of lupus detected by single-photon emission computed tomography. *J Rheumatol* 1993;20:2143–2148.
29. Carette S, Urowitz M, Grossman H, St. Louis E. Cranial computerized tomography in systemic lupus erythematosus. *J Rheumatol* 1982;9:855–859.
30. Steinlin MI, Blaser SI, Gilday DL, et al. Neurologic manifestations of pediatric systemic lupus erythematosus. *Pediatr Neurol* 1995;13:191–197.
31. Awada HH, Mamo HL, Luft AG, Ponsin JC, Kahn MF. Cerebral blood flow in SLE with and without CNS involvement. *J Neurol Neurosurg Psychiatr* 1987;50:1579–1601.
32. Gonzalez-Scarano F, Lisak RP, Bilaniuk LT, Zimmerman RA, Atkins PC, Zweiman B. Cranial computed tomography in the diagnosis of systemic lupus erythematosus. *Ann Neurol* 1979;5:158–165.
33. Grunwald F, Schomburg A, Badali A, Ruhlmann J, Pavics L, Biersack HJ. Eighteen FDG-PET and acetazolamide-enhanced ^{99m}Tc-HMPAO SPECT in systemic lupus erythematosus. *Eur J Nucl Med* 1995;22:1073–1077.

Normal Brain Perfusion Pattern of Technetium-99m-Ethylcysteinate Dimer in Children

Christiaan Schiepers, Alfons Verbruggen, Paul Casaer and Michel De Roo

Department of Nuclear Medicine, Division of Neuro-Pediatrics, University Hospital Gasthuisberg, Leuven, Belgium

The purpose of this study was to assess the normal perfusion pattern of the pediatric brain with ^{99m}Tc-ethylcysteinate dimer (^{99m}Tc-ECD). **Methods:** Tomographic imaging was performed with a dedicated system with high sensitivity and resolution. Sixteen children, referred for brain imaging in the workup of seizure disorder, were included since they turned out negative after a 1-yr follow-up. A standardized brain presentation was obtained after reslicing and reorienting of the three-dimensional volumetric dataset. **Results:** Quantitative analysis did not reveal significant left-right uptake differences per patient. Three age clusters were investigated that showed differences in regional uptake, mainly a relatively increased uptake in basal ganglia, visual and motor cortex. An uptake ratio or perfusion index was calculated after normalization. Normal limits were established for the children in the three groups. **Conclusion:** Technetium-99m-ECD is a safe agent for children and should be the radiopharmaceutical of choice for brain perfusion studies because of favorable radiation dosimetry and stability. The age dependence of perfusion necessitates a database comparison before concluding that the observed perfusion pattern is normal.

Key Words: brain imaging; neuropediatrics; technetium-99m-ethylcysteinate dimer; cerebral blood flow

J Nucl Med 1997; 38:1115–1120

Cerebral blood flow (CBF) or perfusion imaging with ^{99m}Tc-labeled radiopharmaceuticals is a routine procedure in nuclear

medicine clinics. The diagnosis and follow-up of various neurological disorders, such as epilepsy, dementia, stroke and vascular disease, are the main referral indications. Most of the experience over the last year has been obtained with ^{99m}Tc-d,l-HMPAO. Walovitch et al. (1,2) introduced the complex of ^{99m}Tc with L,L-ethylcysteinate dimer (^{99m}Tc-ECD) as an alternative brain perfusion agent. The superior characteristics of ^{99m}Tc for tomographic brain imaging as compared to a radioiodine label, such as in iodoamphetamine (IMP), have been well documented in several reviews (3–5).

The perfusion patterns of ^{99m}Tc-ECD in normal adult volunteers have been reported in multicenter trials by Holman et al. (6) and Vallabhajosula et al. (7). The dosimetric data and biokinetic behavior of the radiopharmaceutical are well known. The main advantages of ^{99m}Tc-ECD over ^{99m}Tc-HMPAO are somewhat higher brain uptake, higher contrast between white and gray matter and greatly increased clearance from the body by the kidneys. The higher concentration available to the brain for first-pass extraction has been demonstrated by Pupi et al. (8). The radiation dose to the brain is slightly higher for ^{99m}Tc-ECD than ^{99m}Tc-HMPAO because of this higher brain uptake. The radiation dose to the other organs is lower, except for the bladder wall. However, an adequate fluid intake and frequent voiding decrease the bladder dose significantly. In a multicenter trial, Lassen and Sperling (9) showed an excellent congruence in CBF measurements between ^{133}Xe and ^{99m}Tc-ECD in the normal as well as the diseased brain, except for early stroke with "luxury" perfusion.

To our knowledge, the normal brain distribution of ^{99m}Tc-ECD in children has not been studied systematically. Brain maturation and perfusion changes with age have been studied by Chiron et al. with ^{133}Xe (10), and Rubinstein et al. with ^{123}I-IMP (11). Chugani et al. (12) evaluated glucose metabolism with ^{18}F-FDG, and investigated the effect of age. In general, there is an increased perfusion and metabolism of the subcortical areas at a young age. Denays et al. (13) studied neonates with ^{99m}Tc-HMPAO and ^{123}I-IMP, and studied brain maturation in very young infants with ^{99m}Tc-HMPAO (14). They found the highest perfusion in sensori-motor zones, visual cortex and striatum.

We were interested in the normal pediatric pattern of ^{99m}Tc-ECD distribution in the brain. For obvious ethical reasons, normal, healthy children and/or their parents cannot be asked to participate. Therefore, we retrospectively reviewed all brain perfusion studies and clinical charts of children referred to nuclear medicine and selected those children who were finally diagnosed as normal, that is free of disease. The children were referred for a ^{99m}Tc-ECD study in the workup for seizure disorder. If epilepsy could be ruled out, their brain perfusion would resemble the pattern of normal healthy children as closely as possible.

MATERIALS AND METHODS

Radiopharmaceutical

L,L-ethylcysteinate dimer dihydrochloride was synthesized according to a published procedure (15). Its identity was confirmed by ^{1}H and ^{11}C NMR spectroscopy and mass spectroscopy. Technetium-99m-ECD was prepared by reconstitution of a homemade lyophilized labeling kit, containing 0.9 mg ECD.2HCl and 0.072 mg SnCl$_2$·2H$_2$O, with 1.85 GBq ^{99m}Tc in the form of sodium pertechnetate in a volume of 3 ml saline, adjusted to pH 7.4 with phosphate buffer. The preparation was analyzed for radiochemical purity using previously published procedures (16).

TABLE 1
Database of Normal Children for Brain Perfusion Imaging with Technetium-99m-ECD

Group	No. of patients	Female	Age (yr) Range	Age (yr) Mean	Age (yr) s.d.
1	5	1	1.3–2.3	1.9	0.5
2	6	2	4.8–8.7	6.7	1.7
3	5	–	10.5–15.4	13.0	2.2
All	16	3	1.3–15.4	7.2	4.8

Patient Preparation

The children were allowed to become accustomed to the room for about 15 min with the lights dimmed. Technetium-99m-ECD with a radiochemical purity over 95%, was administered intravenously in a dose of 10–25 MBq/kg. The acquisition was started 10 min later. Young children were sedated 10–15 min after the tracer administration with a cocktail of Largactil and Luminal intramuscularly (both in a dose of 1 mg/kg) and a pentobarbital suppository (dose 30 mg/kg). This caused an extra delay of 15–30 min.

Acquisition

The images were acquired with a dedicated brain scanner, a single-slice tomograph with 12 detectors. The scanner has a high sensitivity with a resolution of 6 mm FWHM for ^{99m}Tc for the set of collimators used. The patient's head was positioned parallel to the inferior orbito-meatal line and about 8–10 slices were acquired. Slices were acquired sequentially, providing a stack of two-dimensional transaxial images. Acquisition time was 240–300 sec per slice with a relative distance of 10–12 mm. The images were reconstructed with a deconvolution technique and two iterations. Attenuation correction was applied using a best-fitting elliptical contour and constant attenuation coefficient (Chang's method). The attenuation coefficient was determined with a Hoffman brain phantom.

Patients

Between August 1988 and August 1992, all children who were referred for brain perfusion imaging were enrolled. Eighty-eight children had a normal perfusion pattern, as read independently by two experienced nuclear medicine physicians. The clinical charts were also reviewed retrospectively. The perfusion study was finally classified as normal if the child fulfilled the following criteria:

1. EEG was normal at time of admission.
2. Brain CT was normal at time of admission.
3. There was no psycho-motor retardation.
4. The clinical follow-up was negative for 1 yr after admission.

Sixteen patients fulfilled the above conditions, 13 boys and three girls. All studied infants were abnormal and none could be included. The referral indications were seizure disorders, four of which were febrile convulsions (age < 3 yr, Group 1; Table 1). At the time of study, the children were afebrile. Imaging was performed the second week of admission or 1–2 wk later as an outpatient. The children were assigned to three age clusters. Mean age, standard deviation, sex and numbers of the groups are given in Table 1.

Analysis

All eligible studies were reprocessed with commercial software. The transaxial slices were interpolated to a three-dimensional volume set of images in a 128 × 128 × 128 cube. This amounted to a voxel size of 1.6 mm.

To obtain a standardized brain presentation, the data were resampled into 12-mm-thick slices and reoriented along the approximate AC-PC line. Friston et al. (17) have shown an excellent

TABLE 2
Eleven Pairs of Regions Drawn over Ipsi- and Contralateral Cortex, Deep Gray Structures and Cerebellum of Resampled Images

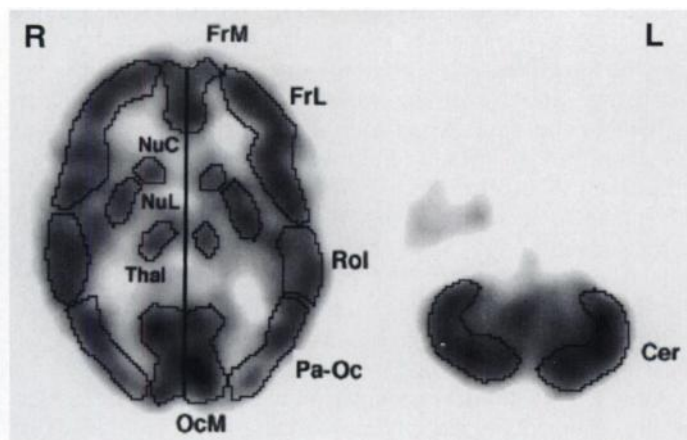| Zone	ROI	Abbreviation
Hemisphere	Both white and gray matter	Hemi
Cortex	Fronto-medial	FrM
	Fronto-lateral	FrL
	Sensory-motor	Rol
	Temporal	Temp
	Parietal/lateral-occipital	Pa-Oc
	Medial-occipital	OcM
Basal ganglia	Caudate nucleus	NuC
	Lentiform nucleus	NuL
Thalamus		Thal
Cerebellum	Hemisphere	Cer

correlation between the AC-PC line on [18]FDG-PET and MR-images, with a deviation of less than 1°. Under normal conditions, this plane through the basal ganglia and thalami easily can be determined on SPECT images.

On the set of standardized brain cuts, regions were drawn manually for further quantitative analysis. Pairs of regions were drawn, as shown in Table 2. The regions of interest (ROIs) were drawn by a technologist with a long experience. Templates were not used, since the size variations with age are considerable. Large ROIs are used for cortex and cerebellum to reduce variability. Frontal and occipital cortex were divided in two, the temporal cortex had one region and the parietal was merged with the lateral occipital. These regions are easy to distinguish and representative examples at two levels are given in Figure 1.
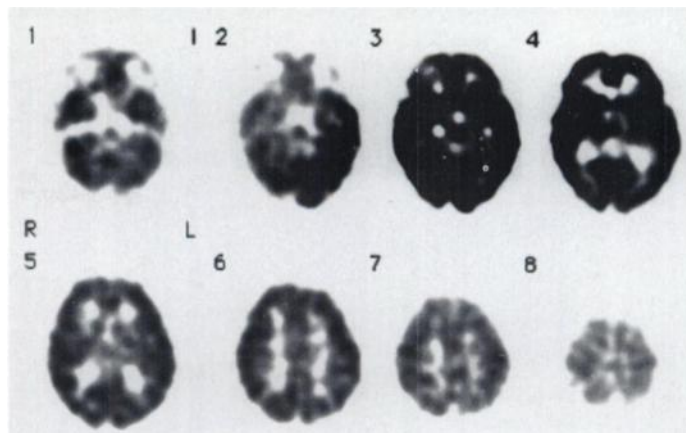
The count density of these regions was analyzed for regional asymmetry. A normalization to the cerebellum or cortex was performed to provide a perfusion index and compare regional uptake between patients. First we calculated the average uptake per ROI over all the image slices, in other words, weighting of the count density to the area involved for each ROI. This provides 11 pairs of values, from which the perfusion indices can be calculated.

Statistics

Results are expressed as the average number of counts per pixel in each region or perfusion index. Left-to-right ratios were computed to evaluate regional changes. Paired Student's t-tests were applied to evaluate the differences between these parameters, and a value of $p < 0.05$ was considered significant. An analysis of variance (ANOVA) was performed on perfusion indices.

FIGURE 2. Transaxial slices of the resampled and reoriented dataset of a 2-yr-old child. The highest uptake is in the basal ganglia and visual cortex. Note the prominent brain stem on slices 1 and 2.

RESULTS

In Figures 2 and 3, two typical examples of the final standardized brain perfusion pattern are shown. The images of the younger child (Fig. 2) show a small increase of ^{99m}Tc-ECD uptake in the basal ganglia when compared to the teenager's images (Fig. 3).

There were no statistically significant differences between similar regions in the right and left hemisphere. Therefore, ipsi- and contralateral ROI results were averaged. The maximum uptake difference between corresponding left and right sided ROIs was 12% and was over 10% in four children on five occasions: three times in Group 1, twice in Group 2 and none in Group 3. In Figures 4 and 5, the results are given for the three age groups after normalization to the cerebellum and cortex, respectively. In both figures, the highest uptake ratio or perfusion index is found for the medial occipital cortex and for the striatum. The influence of age is clearly different for the two normalization methods. Normalization to the cerebellum (Fig. 4) reveals the highest uptake in the medial occipital cortex and basal ganglia of Group 1, and the differences between Groups 1 and 3 are significant. After normalization to the cortex (Fig. 5), the trend with age reverses for the medial occipital zone. The age trend for the striatum remains, but is less pronounced. Note the clear increase of cerebellar uptake, relative to the cortex, with age.

FIGURE 1. Representative planes with the ROIs. The higher level through the basal ganglia has all ROIs of Table 2 except the cerebellum and temporal cortex. The lower level plane shows the cerebellar hemispheres.
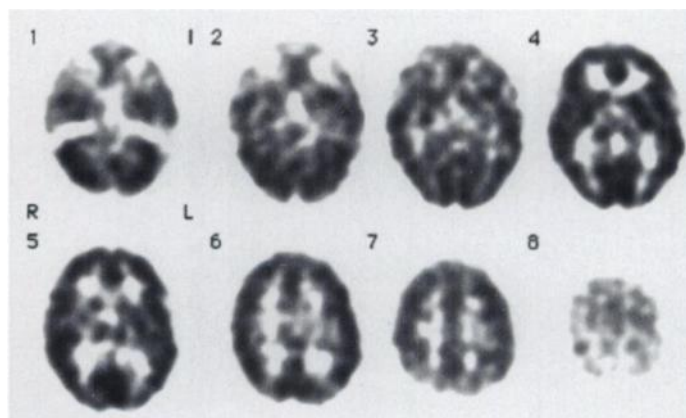

FIGURE 3. Final set of resampled and reoriented transverse images of a 13-yr-old. Because of the rotation in the sagittal plane, the posterior portion at the highest level has fewer counts. The top slice is not 12 mm, leading to a lower total count and corresponding intensity of slice 8. Note the larger size of the brain when compared to Figure 2 and the somewhat lower uptake of the basal ganglia relative to the visual cortex.
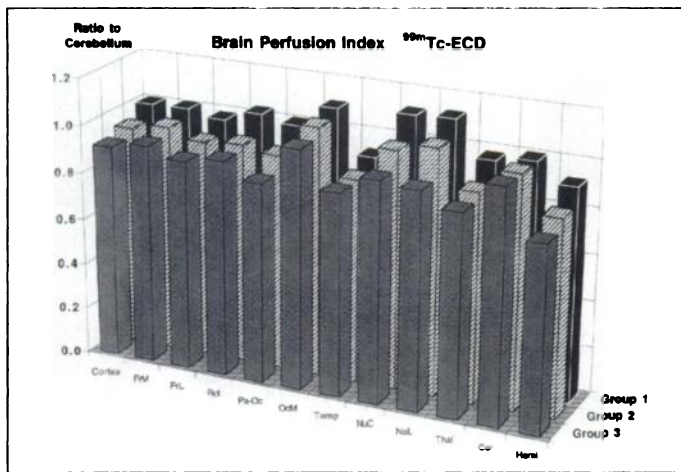
FIGURE 4. Perfusion indices of the three different age groups. Average uptake values have been normalized to the cerebellum. Note the clear decrease in the striatum (caudate and lentiform nuclei) as the age increases. The medial occipital ROI has the highest uptake, except for Group 1 where the striatum is maximal, in part related to the open eyes during ^{99m}Tc-ECD injection. See Table 2 for the abbreviations.

The ANOVA did not reveal significant changes between left and right hemispheres (p = 0.12). The effect of age group and ROI were both significant after normalization to the cerebellum (p = 0.03 and p < 0.0001, respectively), and the interaction was significant (p < 0.0001). After normalization to the cortex the effect of age group was no longer significant (p = 0.6), whereas ROI still was (p < 0.0001). However, the interaction between age group and region was still significant (p < 0.0001). This analysis corroborates a dependence of age with the regional perfusion pattern observed.

The mean perfusion index and s.d. per ROI, in each hemisphere, are given in Table 3 for the three groups in digits (Table 3) and as graphical displays (Fig. 6), after normalization to the average cerebellar uptake. The perfusion indices of the above selected normal children are used for reference in a database. Thus, perfusion patterns of new pediatric patients can be compared to one of the three available age groups. The medial occipital cortex has the highest index, corresponding to the highest uptake. Relative hyperperfusion of the frontal cortex is seen at older age (Group 3, Table 3, Fig. 6), giving the slightly higher values in the frontal compared to parietal and temporal zones.
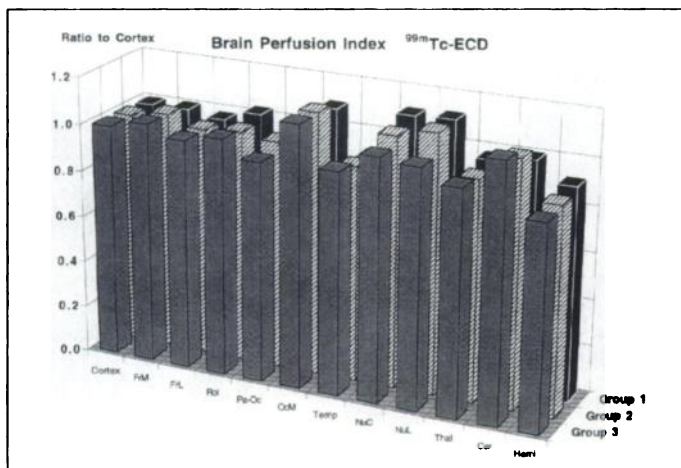
FIGURE 5. Perfusion indices of the three different age groups. Average uptake values have been normalized to the cortex, in other words the weighted average of all gray matter. Compared to Figure 4, the age dependence of the medial occipital ROI has reversed. The cerebellar perfusion index increases with age. See Table 2 for abbreviations.

DISCUSSION

In this study, the normal pediatric perfusion pattern for ^{99m}Tc-ECD was evaluated retrospectively in 16 children. These children were negative patients, referred during the workup of seizure disorder. They are considered to represent the normal pediatric brain pattern, in other words the distribution of ^{99m}Tc-ECD in children at various ages. For this survey, 88 perfusion studies were reviewed in detail and none of these children experienced adverse reactions from the radiopharmaceutical.

Several differences exist between ^{99m}Tc-ECD and the more frequently used ^{99m}Tc-HMPAO. The radiation dose to the bladder by ^{99m}Tc-ECD (5,6) is somewhat higher due to faster excretion, but may be reduced by urging the children to drink and void frequently. The low in-vitro stability of ^{99m}Tc-HMPAO is a major disadvantage, especially if rapid injections are required as in ictal epilepsy imaging. Different methods for stabilization of ^{99m}Tc-HMPAO have been reported (18), but none of the proposed methods presently is approved in Europe. Technetium-99m-ECD uptake was reportedly more linear with CBF than with ^{99m}Tc-HMPAO, indicating less backdiffusion of tracer from the brain to the vascular space (19). However, uptake mechanisms of ^{99m}Tc-ECD are definitely different from those of ^{99m}Tc-HMPAO (2,20). The so-called "luxury" perfusion pattern is not present with ^{99m}Tc-ECD (9) and, in general, uptake appears slower than with ^{99m}Tc-HMPAO, as has been demonstrated with ictal perfusion studies (21). However, Biersack et al. (21) have shown that ^{99m}Tc-ECD is an effective marker for perfusion imaging in epilepsy and can be used both for ictal and interictal studies. Therefore, we are strongly in favor of ^{99m}Tc-ECD as the radiopharmaceutical of choice for neuropediatric patients.

Since we were interested in comparing the perfusion patterns of children, we did not want to depend on differences in dose administered, delay interval before the acquisition (in case of sedation), acquisition duration or individual uptake variability. Therefore, a normalization step was necessary. The uptake ratio or perfusion index is usually calculated relative to the cerebellum (Figs. 4 and 6, Table 3). We have observed that for young children (<2 yr) this does not seem to be the optimal way. Apparently, the maturation rate of the cerebellum is different from that of the cortex at a young age, leading to quite different regional perfusion indices.

The s.d. of the perfusion index for individual ROIs varied between 0.01 and 0.09, in other words less than 10%, except for the caudate nucleus in Group 1 that bilaterally had values of 0.15. Given the small size of these structures at this age and the limited resolution of our system, the effect of the partial volume is the greatest. This caused the largest variations depending on how the structures are 'cut' in the image planes, which is not surprising. Because of the partial volume effect, the actual activity in the basal ganglia is higher in young children as compared to teenagers, amplifying the age trend in perfusion differences. Correction techniques for these effects, however, are cumbersome and complicated and were not available to us.

Matsuda et al. (22) have shown in adults that the perfusion indices obtained with ^{99m}Tc-ECD were the same as those obtained with ^{99m}Tc-HMPAO, and could easily be converted to CBF values in ml/100 g/min based on ^{133}Xe studies. Thus, CBF measurements with ^{99m}Tc-ECD seem feasible.

Although we did not encounter problems with the early start of the acquisition, present knowledge of the biokinetics of ^{99m}Tc-ECD suggests that a 10-min delay is too short and an interval of at least 30 min between dose administration and onset of acquisition is recommended (3,5,20). In this series of
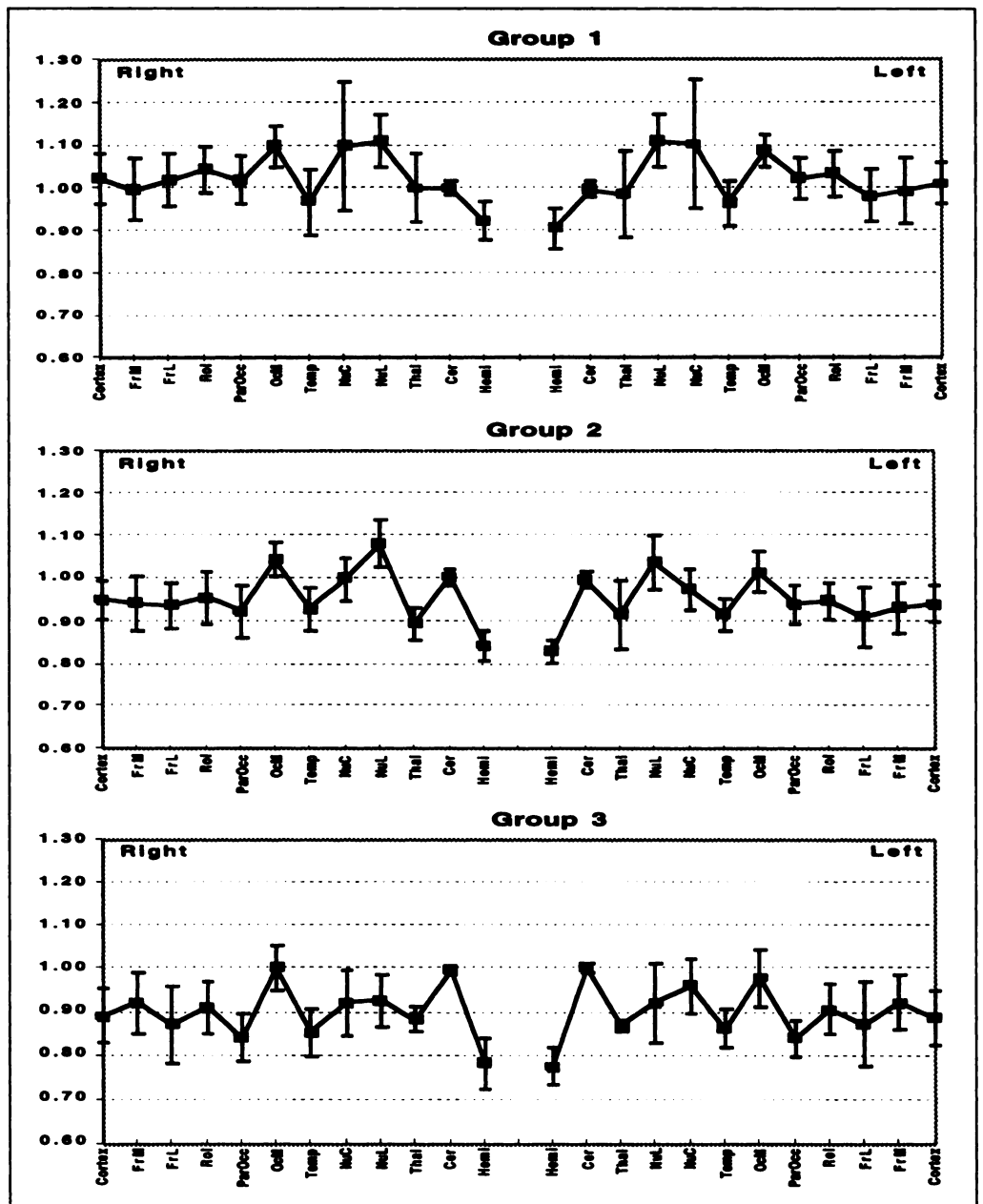
FIGURE 6. Average perfusion index with upper and lower limits (± 1 s.d.) for the various regions (see Table 2 for abbreviations). The values are given for the hemispheres from right to left in a cyclical way: cortical, basal ganglia, thalamus, cerebellum and reversed. Normalization was done to the average cerebellar count rate. Separate graphs are given for the three age clusters: Groups 1, 2 and 3.

patients, such a 30-min delay was present only for Group 1 and other children who needed to be sedated.

CONCLUSION

Technetium-99m-ECD is a safe radiopharmaceutical for brain imaging in pediatric patients. Radiation dose is acceptable and compares favorably to that of other available agents. The perfusion pattern is different for toddlers than for teenagers; younger children have preferential perfusion of the basal ganglia, visual and motor cortex. The age dependence necessitates quantification in order to conclude that the perfusion is normal. A database of perfusion indices with standard deviation is presented for three age clusters.

TABLE 3
Average Perfusion Index and Standard Deviation per ROI

Group	Right FroM	FroL	Rol	PaOc	OcM	Temp	NuC	NuL	Thal	Right Cer	Left Cer	Thal	NuL	NuC	Temp	OcM	PaOc	Rol	FrL	Left FrM
1 avg.	0.997	1.020	1.045	1.021	1.097	0.969	1.098	1.112	1.002	1.001	0.999	0.988	1.112	1.103	0.967	1.089	1.023	1.034	0.984	0.994
s.d.	0.072	0.062	0.053	0.056	0.048	0.076	0.148	0.060	0.081	0.016	0.016	0.102	0.061	0.148	0.055	0.038	0.046	0.052	0.060	0.075
2 avg.	0.942	0.937	0.954	0.923	1.043	0.927	0.998	1.080	0.894	1.004	0.996	0.914	1.038	0.974	0.914	1.015	0.938	0.947	0.910	0.930
s.d.	0.063	0.053	0.059	0.060	0.041	0.052	0.050	0.055	0.037	0.017	0.017	0.079	0.065	0.049	0.039	0.047	0.045	0.041	0.070	0.060
3 avg.	0.921	0.871	0.909	0.841	1.002	0.852	0.920	0.925	0.884	0.998	1.002	0.868	0.921	0.959	0.862	0.979	0.840	0.906	0.872	0.921
s.d.	0.072	0.091	0.061	0.054	0.054	0.057	0.077	0.061	0.028	0.010	0.010	0.010	0.091	0.063	0.045	0.065	0.044	0.057	0.097	0.062

The values are given for each hemisphere of the three age clusters. Data are ordered in a cyclical way: cortical, basal ganglia, thalamus, cerebellum and reversed. Normalization was done to the average cerebellar count rate. See Table 2 for abbreviations.

REFERENCES

1. Walovitch RC. Hill TC, Garrity ST, et al. Characterization of technetium-99m-L,L-ECD for brain perfusion imaging. Part 1: pharmacology of technetium-99m-ECD in nonhuman primates. *J Nucl Med* 1989;30:1892–1901.
2. Walovitch RC, Franceschi M, Picard M, et al. Metabolism of ^{99m}Tc-L,L-ethyl-cysteinate dimer in healthy volunteers. *Neuropharmacology* 1991;30:283–292.
3. Lassen NA. Imaging brain infarcts by single-photon computed emission tomography with new tracers. *Eur J Nucl Med* 1994;21:189–190.
4. Saha GB, MacIntyre WJ, Go RT. Radiopharmaceuticals for brain imaging. *Semin Nucl Med* 1994;24:324–349.
5. Verbruggen AM. Radiopharmaceuticals: state of the art. *Eur J Nucl Med* 1990;17:346–364.
6. Holman BL, Hellman RS, Goldsmith SJ, et al. Biodistribution, dosimetry and clinical evaluation of technetium-99m-ethyl cysteinate dimer in normal subjects and in patients with chronic cerebral infarction. *J Nucl Med* 1989;30:1018–1024.
7. Vallabhajosula S, Zimmerman RE, Picard M, et al. Technetium-99m-ECD: a new brain imaging agent: in vivo kinetics and biodistribution studies in normal human subjects. *J Nucl Med* 1989;30:599–604.
8. Pupi A, Castagnoli A, De Cristofaro MT, Bacciottini L, Petti AR. Quantitative comparison between ^{99m}Tc-HMPAO and ^{99m}Tc-ECD: measurement of arterial input and brain retention. *Eur J Nucl Med* 1994;21:124–130.
9. Lassen NA, Sperling B. Technetium-99m-bicisate reliably images CBF in chronic brain diseases but fails to show reflow hyperemia in subacute stroke: report of a multicenter trial of 105 cases comparing ^{133}Xe and ^{99m}Tc-bicisate (ECD, neurolite) measured by SPECT on same day. *J Cereb Bl Flow Metab* 1994;14:S44–S48.
10. Chiron C, Raynaud C, Maziere B, et al. Changes in regional cerebral blood flow during brain maturation in children and adolescents. *J Nucl Med* 1992;33:696–703.
11. Rubinstein M, Denays R, Ham HR, et al. Functional imaging of brain maturation in humans using iodine-123-iodoamphetamine and SPECT. *J Nucl Med* 1989;30:1982–1985.
12. Chugani HT, Phelps ME, Mazziotta JC. Positron emission tomography study of human brain function development. *Ann Neurol* 1987;22:487–497.
13. Denays R, Pachterbeke T, Tondeur M, et al. Brain single-photon emission computed tomography in neonates. *J Nucl Med* 1989;30:1337–1341.
14. Denays R, Tondeur M, Foulon M, et al. Regional brain blood flow in congenital dysphasia: studies with technetium-99m-HMPAO SPECT. *J Nucl Med* 1989;30:1825–1829.
15. Blondeau P, Berse C, Gravel D. Dimerization of an intermediate during the sodium in liquid ammonia reduction of L-thiazolidine-4-carboxylic acid. *Can J Chem* 1967;45:49–52.
16. Van Nerom C, Bormans G, Crombez D, De Roo M, Verbruggen A. Radiochemical analysis of ^{99m}Tc-ECD by TLC and HPLC. In: Nicolini M, Bandoli G, Mazzi U, eds. *Technetium and rhenium in chemistry and nuclear medicine 3*. Verona, Italy: Cortina Int.; 1990:525–529.
17. Friston KJ, Passingham RE, Nutt JG, et al. Localization in PET images: direct fitting of the intercommissural (AC-PC) line. *J Cereb Blood Flow Metab* 1989;9:690–695.
18. Mang'era KO, Vanbillioen HP, Schiepers CW, Verbruggen AM. Stabilization of high-activity ^{99m}Tc-d,l-HMPAO preparation with cobalt chloride and their biological behaviour. *Eur J Nucl Med* 1995;22:1163–1172.
19. Friberg L, Andersen AR, Lassen NA, Holm S, Dam M. Retention of ^{99m}Tc-bicisate in the human brain after intracarotid injection. *J Cereb Bl Flow Metab* 1994;14:S19–S27.
20. Walovitch RC, Cheesman EH, Maheu LJ, Hall KM. Studies of the retention mechanism of the brain perfusion imaging agent. Technetium-99m-bicisate (^{99m}Tc-ECD). *J Cereb Blood Flow Metab* 1994;14:S4–S11.
21. Grunwald F, Menzel C, Pavics L, et al. Ictal and interictal brain SPECT imaging in epilepsy using technetium-99m-ECD. *J Nucl Med* 1994;35:1896–1901.
22. Matsuda H, Yagishita A, Tsuji S, Hisada K. A quantitative approach to technetium-99m-ethylcysteinate dimer: a comparison with technetium-99m-hexamethylpropylene amine oxime. *Eur J Nucl Med* 1995;22:633–637.

Brain Perfusion SPECT in Lyme Neuroborreliosis

Hisashi Sumiya, Katsuji Kobayashi, Chikako Mizukoshi, Tatsuyuki Aoki, Yoshifumi Koshino, Junichi Taki and Norihisa Tonami

Departments of Nuclear Medicine and Psychiatry, Kanazawa University School of Medicine, Kanazawa, Japan

SPECT imaging brain perfusion using ^{99m}Tc-HMPAO was performed on a 38-yr-old woman with Lyme neuroborreliosis confirmed by autopsy. The patient had been suspected of spinocerebellar degeneration. Cerebral blood flow was diffusely decreased throughout cerebral cortices but cerebellar blood flow was not impaired, which indicated that the diagnosis was unlikely spinocerebellar degeneration. These findings suggested that brain perfusion SPECT provides useful information in diagnosing the patients with Lyme neuroborreliosis, especially when spinocerebellar degeneration is included in the differential diagnosis.

Key Words: Lyme neuroborreliosis; SPECT; HMPAO; spinocerebellar degeneration

J Nucl Med 1997; 38:1120–1122

Lyme disease is a multisystemic disease caused by tick-borne spirochete Borrelia burgdorferi, and its invasion into the central nervous system develops a diversity of neurologic and psychiatric disturbances (*1,2*). In Lyme disease, the central nervous system involvement usually becomes involved in the second stage showing meningitis, multiple cranial nerve palsy, motor or sensory radiculoneuritis and polyneuropathy. In more severely affected cases, disseminated cerebromyelitis, leukoencephalitis and demyelinating encephalopathy have been found, which characterize the third stage of Lyme disease, known as Lyme neuroborreliosis (LNB). Findings in imaging studies with brain CT and MRI are frequently subtle and nonspecific (*3,4*).

This article describes previously unreported HMPAO-SPECT findings in a patient with LNB.

CASE REPORT

A woman, who had been in good health, became aware of unstable walking at 37 yr. She had not experienced any signs or symptoms of skin lesion or joint pain. She consulted a general hospital and was neurologically examined, but no abnormality was detected. However, her neurological symptoms gradually developed. Her gait became definitely ataxic, and she could not stand up for a long time. She had choreoathetotic movement in her upper extremities, spoke explosively and had dysdidochokinesis. Five months later, she could not stand up and memory disturbance became evident with inertia, and she was admitted to our hospital.

Neurological examination disclosed marked disturbance in coordination and dysmetria including intentional tremors. She was frequently drowsy, restless and disorientated as to time and place. She responded very slowly to any questions. No meningeal signs were detected. Mini-Mental State Examination score was 16/30 (*5*). Her ocular movements had limitation on upward and downward gaze. Her pupil was miotic but reactive. She was judged to have supranuclear bulbar palsy because of the absence of pharyngeal reflex. She had muscle weakness detected in general skeletal muscles that were hypotonic. Choreoathetotic movements were present in her upper and lower extremities. Deep tendon reflexes